Vortex Flow in a Convergent–Divergent Nozzle

Andrew D. Cutler*
George Washington University, Hampton, Virginia 23681-2199
and
Richard W. Barnwell†
Virginia Polytechnic Institute and State University, Hampton, Virginia 23666-1568

Introduction

In certain geometries, supersonic swirling jets mix more rapidly (in a shorter axial distance) with the surrounding gas than nonswirling jets and, thus, may find application in the fields of combustion and propulsion. Experiments in which pressure-matched supersonic swirling jets discharged into stagnant air demonstrated greater mixing layer growth rate in the near field, which could be correlated with mean streamline curvature.[1,2] These studies also found that, if the jets were operated overexpanded, vortex breakdown occurred, leading to a substantial increase in mixing. A later study considered the injection of a supersonic swirling jet at 30 deg into a supersonic duct flow.[3] Other work includes that of Naughton et al.[4] and the references quoted therein. Critical to the implementation of the studies in Refs. 1–3 was the development of a simple, approximate method for the calculation of the flow of a vortex in an axisymmetric nozzle. This method assumes steady, quasi-one-dimensional (negligible radial velocity), irrotational, isentropic flow with a line vortex (singularity) on the axis and (it was subsequently found) is equivalent, in many respects, to the method of Mager.[5] The purpose of this Note is to present the method and to establish its validity in this application by comparing the results of calculations to those of experiment.

Method

Nomenclature used in this analysis is conventional, with the superscript $*$ denoting the sonic condition (the condition attained in flowing isentropically to a velocity with magnitude equal to the sonic velocity). Because the flow is irrotational and quasi one dimensional, the circumferential velocity is given by $v_\theta \equiv a^* R/r$, where r is the radius, R serves as a characteristic radius (physically, the radius at which the circumferential velocity equals the sonic velocity when other components of velocity are zero), and a^* is the sonic speed of sound. It also follows from these assumptions that the axial velocity u is a function only of axial distance x. The circulation of the vortex is $\Omega = 2\pi a^* R$. A dimensionless mass flow rate in the nozzle is

$$\phi \equiv \frac{\dot{m}}{\rho^* a^* R^2} = \int_{\eta_i}^{\eta_w} \frac{\rho}{\rho^*} M_x^* \pi \, \mathrm{d}\eta^2 \equiv \text{const} \tag{1}$$

where $\eta \equiv r/R$ and $M_x^* \equiv u/a^*$. The lower limit of integration is described subsequently; the upper limit is the wall of the nozzle. The density is eliminated from Eq. (1) using the energy equation for isentropic flow:

$$\rho/\rho^* = \{[(\gamma+1)/2] - [(\gamma-1)/2]M^{*2}\}^{1/(\gamma-1)} \tag{2}$$

$$M^{*2} \equiv \frac{v_\theta^2 + u^2}{a^{*2}} = \frac{1}{\eta^2} + M_x^{*2} \tag{3}$$

It is clear from Eqs. (2) and (3) that, as $\eta \to \eta_i$ from above, the density and also pressure and temperature go to zero, where

$$\eta_i \equiv \left\{[(\gamma+1)/(\gamma-1)] - M_x^{*2}\right\}^{-\frac{1}{2}} \tag{4}$$

The only physically possible solution in the region $0 < \eta < \eta_i$ [where Eq. (4) gives an imaginary number] is zero density; consequently, η_i is taken as the lower limit of integration for the mass flow rate. Evaluation of the wall radius η_w as a function of M_x^* for various constant ϕ shows that, for all $\phi > 0$, the acceleration of an irrotational, vortical flow to high axial speeds requires a convergent–divergent nozzle. Conditions at the throat (minimum radius, subscript t) of the nozzle may be found by differentiating Eq. (1) [after substitution of Eqs. (2) and (3)] with respect to M_x^* at constant η_w and setting the result to zero. This results in the following equation relating $\eta_{w,t}$ to $M_{x,t}^*$:

$$\int_{\eta_{i,t}}^{\eta_{w,t}} \left(\frac{\gamma+1}{\gamma-1} - M_{x,t}^{*2} - \frac{1}{\eta^2}\right)^{(2-\gamma)/(\gamma-1)} \times \left[1 - M_{x,t}^{*2} - \frac{\gamma-1}{(\gamma+1)\eta^2}\right] \mathrm{d}\eta^2 = 0 \tag{5}$$

Note that $M_{x,t}^*$ is found to tend to 1 from below as $\eta_{w,t} \to \infty$, the case of no swirl.

The experimental apparatus described by Cutler et al.[2] is shown in Fig. 1. Air is injected at low speed ($M < 0.2$) from the plenum through up to 96 tangentially drilled holes into the swirl chamber. All of the injected air enters the swirl chamber at the same radius and with the same tangential velocity and entropy, producing an irrotational vortex in the chamber with perhaps a rotational core on the axis due to the effects of viscosity. The air exits the swirl chamber through a convergent–divergent nozzle and discharges to the atmosphere as a jet. By interchanging end pieces, the height of the swirl chamber L, and consequently the number of injection holes exposed, may be varied. Decreasing the number of injection holes increases the tangential velocity of injection, thus increasing the vortex circulation. By removing the end piece altogether, the nozzle can be run without a vortex.

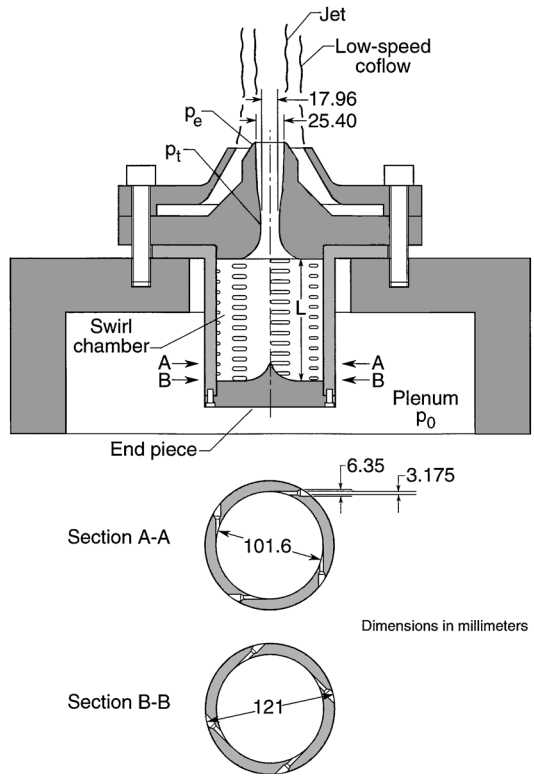

Fig. 1 Experimental nozzle.

Received 24 January 1999; revision received 26 April 1999; accepted for publication 19 May 1999.

*Associate Professor, Joint Institute for the Advancement of Flight Sciences. Senior Member AIAA.

†Professor, Virginia Consortium of Engineering and Science Universities. Fellow AIAA.

The mass flow in the nozzle equals the mass flow through the tangentially drilled injection holes, so that $\rho_j A_j v_{\theta,j} = \phi \rho^* a^* R^2$, where subscript j refers to tangential injection quantities and A_j is the total area of the tangential injection holes. By using $v_{\theta,j} r_j \equiv a^* R$, this may be rewritten as

$$\frac{A_j}{r_{w,t}^2} = \phi \frac{\rho^*}{\rho_j} \frac{\eta_j}{\eta_{w,t}^2} \tag{6}$$

The density ratio is eliminated from Eq. (6) in terms of η_j using Eqs. (2) and (3) and setting $M^*_{x,j} = 0$, that is, assuming the axial component of velocity is zero at the tangential injection holes.

The solution procedure is to first specify $M^*_{x,t}$, the normalized axial throat velocity, and then solve Eq. (5) by integrating numerically, starting from $\eta_{i,t}$ and advancing η in small increments until the integral equals zero (again), at which point $\eta = \eta_{w,t}$. Then Eq. (1) [after substitution of Eqs. (2) and (3)] is integrated numerically at the throat to obtain ϕ. Given $\eta_{w,t}$ and the geometrically specified $r_{w,t}$ and r_j, we can find η_j from $R = r_{w,t}/\eta_{w,t}$, $\eta_j = r_j/R$. Then A_j can be calculated from Eq. (6). If A_j is specified rather than $M^*_{x,t}$, the procedure is to iterate upon $M^*_{x,t}$ until the specified and calculated values of A_j agree. The value of M^*_x at the exit of the nozzle (subscript e) can be found given $r_{w,e}$ by iterative solution of Eq. (1) applied at the exit. From this, all other quantities at the exit are easily obtained as a function of the radius.

Results

The results described by Cutler et al.[2] include surveys at the nozzle exit utilizing cone static pressure, five-hole pressure, and total temperature probes. These probe results, when taken together, allowed various quantities such as Mach number, static pressure, total pressure, temperature, and density to be derived. In addition, wall static pressure measurements were made using static taps located in the plenum, at the throat, and at the exit of the nozzle. Three cases are described: the straight case in which there was no swirl in the nozzle (end piece removed), the low-swirl case, and the high-swirl case. According to Cutler et al.,[2] the data for v_θ/u at the nozzle exit can be fitted to the function K/r in the outer part of the jets (consistent with irrotational flow), where K, a measure of the swirl strength, is $0.144 d_e$ for the low-swirl case and $K = 0.209 d_e$ for the high-swirl case. The tangential injection area A_j, and $M^*_{x,t}$, R, ϕ, and $M^*_{x,e}$ from the calculation were, respectively, for the low-swirl case 760 mm^2, 0.927, 5.68 mm, 4.27, and 1.747 and for the high-swirl case 127 mm^2, 0.806, 10.71 mm, 0.372, and 1.777. Figure 2 shows the experimental ratios of throat and exit wall static tap pressure to plenum pressure (subscript 0) and the corresponding calculated

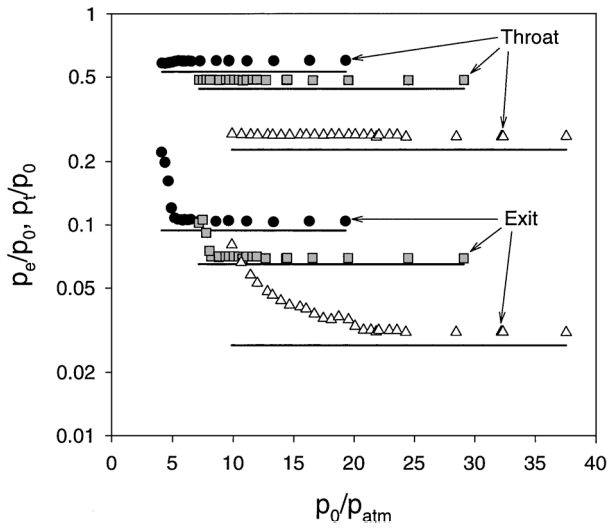

Fig. 2 Comparison between experimental and calculated ratios of throat and exit wall static pressure to plenum pressure as a function of plenum pressure: ●, no swirl; ■, low swirl; △, high swirl; and ——, calculation.

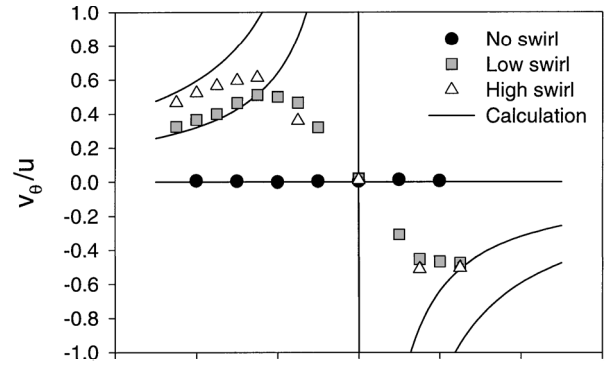

a) Ratio of tangential to axial velocity

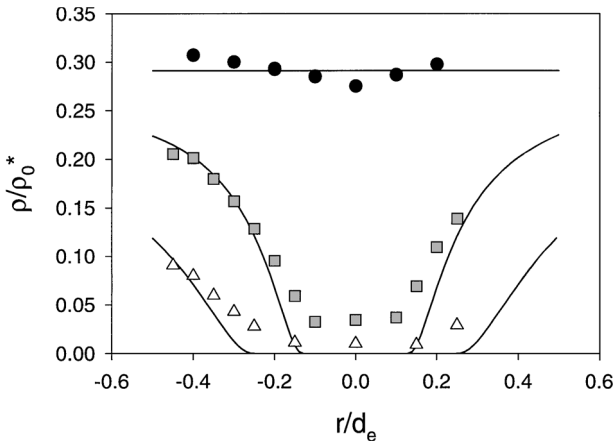

b) Ratio of density to plenum sonic density

Fig. 3 Comparison between probe measurements at the nozzle exit and the calculations.

pressures plotted against the ratio of plenum pressure to atmospheric pressure. In all cases, as the plenum pressure is raised with respect to atmospheric pressure, the wall pressures asymptote to constant values, indicating no downstream influence. Asymptotic pressures are roughly 10% higher than the calculation at both the throat and exit for all cases. These discrepancies are presumably due to viscous effects and/or to failure of the assumption of quasi-one-dimensional flow; the flow at the throat was probably not one dimensional due to surface curvature and at the exit was probably only roughly one dimensional because the nozzle contour was designed using arbitrarily chosen smooth curves rather than, for example, the method of characteristics. Nozzle exit survey results presented in Ref. 2 show that in the no-swirl case the total pressure equals the plenum pressure across the whole diameter, whereas in the swirl cases, the total pressure falls to close to zero at the axis and is below the plenum pressure for about 0.5 (low swirl) or 0.6–0.7 (high swirl) of the diameter, indicating a large viscous core. Additionally, in the no-swirl case the total temperature equals the plenum temperature, whereas in the swirl cases, it falls to as low as 75% of the plenum temperature in the core region. These and other experimental results, including those for tangential velocity and density (normalized with plenum sonic rather than local sonic density), which are shown in Fig. 3, agree approximately with the calculations in the no-swirl case and in the swirl cases in the region surrounding the core (within 10–15%), although large discrepancies exist within the core. Therefore, in the swirl cases the flow surrounding the core is approximately irrotational and isentropic, and the vortex has approximately the predicted circulation (within 10–15%). The circulation can be predicted despite errors in the core region because the core region is a region of low density and occupies a smaller fraction of the flow area than of the nozzle diameter. Thus, a large core with large relative errors produces smaller errors in the integrated nozzle mass flow rate, and the effect of the core on the velocity of tangential injection

into the swirl chamber, and consequently on the vortex circulation, therefore, is also smaller. Indeed, in the experiment of Kraus and Cutler[3] using similar nozzle geometries, measured mass flow rates and rates calculated based on plenum conditions using the present method agreed within 8%.

Conclusion

A simple analytical method for the design of convergent–divergent nozzles that produce axisymmetric vortex flows has been presented. The method assumes compressible, isentropic, quasi-one-dimensional flow. Experimental results confirm the applicability of the method and give an indication of the errors due to viscous effects at the core.

References

[1]Levey, B. S., "An Experimental Investigation of Supersonic Vortical Flow," M.S. Dissertation, School of Engineering and Applied Science, George Washington Univ., Hampton, VA, 1991.

[2]Cutler, A. D., Levey, B. S., and Kraus, D. K., "Near-Field Flow of Supersonic Swirling Jets," *AIAA Journal*, Vol. 33, No. 5, 1995, pp. 876–881.

[3]Kraus, D. K., and Cutler, A. D., "Mixing of Swirling Jets in a Supersonic Duct Flow," *Journal of Propulsion and Power*, Vol. 12, No. 1, 1996, pp. 170–177.

[4]Naughton, J. W., Cattafesta, L. N., III, and Settles, G. S., "An Experimental Study of Compressible Turbulent Mixing Enhancement in Swirling Jets," *Journal of Fluid Mechanics*, Vol. 330, 1997, pp. 271–305.

[5]Mager, A., "Approximate Solution of Isentropic Swirling Flow Through a Nozzle," *ARS Journal*, Vol. 31, Aug. 1961, pp. 1140–1148.

R. M. C. So
Associate Editor

Structural Damage Detection Using the Simulated Evolution Method

Dar-Yun Chiang* and Wen-Yi Lai†
National Cheng-Kung University, Tainan 701, Taiwan, Republic of China

Introduction

SYSTEM identification methods have been extensively employed in recent years for structural damage assessment.[1,2] The theoretical background of system identification methods is that the departure of the measured response from analytically predicted values can be used to identify changes in system parameters such as elements of stiffness matrix, which in turn reflect possible structural damage. Most system identification methods, which are formulated by the output-error method or the equation-error method, essentially result in unconstrained or constrained optimization problems.[3] The major problems associated with such optimization-based approaches include the loss of physical connectivity associated with a model and the overparameterization of an analytical model, which may result in the problem of identifiability, that is, lack of uniqueness in the identified parameter values.

Berman[4,5] pointed out that there is no unique valid linear discrete model to be identified using limited data obtained from a dynamic test. To alleviate the problem of identifiability, a two-stage damage detection approach has been proposed.[6,7] In the first stage, the residual force method is employed to locate candidate damage parts in a structural system; in the second stage, the damage extent of the candidate damage parts is then evaluated using an optimization method. The residual force method is effective in damage localization using insuffucient modal data as long as the modeling error is small for the undamaged structure.[7,8] Once the location of possible damage in a structural system is identified, the damage extent is further evaluated using an optimization method. In the present study, we employ the method of simulated evolution, which is a global optimization method and has the capability of locating multiple global optima within a specified domain.[9,10] By using the global optimization method, we can ensure that some or all of the possible damage scenerios, if theoretically nonunique results do exist, can be found in the second stage for further assessment.

Two-Stage Damage Detection Method

To effectively reduce the number of parameters to be identified and to alleviate the problem of lack of uniqueness in the result of structural damage analysis, a two-stage structural damage detection method is employed.

In the first stage of damage localization, the aim is to locate possible damage areas so that the damage extent can be estimated more reliably in a separate stage. In this study, the residual force method[7,8] is employed. By assuming that the mass matrix $\boldsymbol{M}$ is unchanged as damage occurs, we introduce the relation

$$\boldsymbol{K}_d = \boldsymbol{K}_0 + \Delta\boldsymbol{K} \tag{1}$$

where $\boldsymbol{K}_d$ and $\boldsymbol{K}_0$ are the stiffness matrices associated with the damaged and undamaged structural models, respectively, and $\Delta\boldsymbol{K}$ is the corresponding changes. Define the residual force vector $\boldsymbol{R}_i$ of the ith mode as

$$\boldsymbol{R}_i \equiv \left(\boldsymbol{K}_0 - \omega_d^2\boldsymbol{M}\right)\phi_{di} = -\Delta\boldsymbol{K}\phi_{di} \tag{2}$$

where ω_{di} and ϕ_{di} are, respectively, the ith modal frequencies and mode shapes of the structure after damage occurs. The second equality in Eq. (2) follows from Eq. (1) and the eigenequations associated with the structural system after damage. By inspecting Eq. (2) it can be seen that the residual force vector $\boldsymbol{R}_i$ will have only nonzero elements at the degrees of freedom (DOFs) affected by damage (nonzero elements in $\Delta\boldsymbol{K}$). It is remarkable that the residual force vector $\boldsymbol{R}_i$ can be determined directly using the known analytical model (must be accurate enough) and the measured postdamage eigendata for any mode available, as shown in Eq. (2).

In the second stage, the candidate damaged elements (or substructures) are further evaluated to determine their damage extent. To reduce effectively the number of parameters while retaining physical connectivity of the model, we introduce reparameterization of the stiffness matrix as follows:

$$\boldsymbol{K}_d = \boldsymbol{K}_0 + \Delta\boldsymbol{K} = \boldsymbol{K}_0 - \sum_{i=1}^{N_d}\theta_i\boldsymbol{K}_i \tag{3}$$

where N_d is the number of possibly damaged elements (or substructures) that are identified in the first stage and θ_i, $i = 1 \sim N_d$, are the corresponding damage parameters. The value of θ_i is 1 if the ith element is completely damaged and $\theta_i = 0$ if the ith element is not damaged at all.

To identify the damage parameters associated with those elements that are possibly damaged, the least-squares output-error method[10] is employed. In this study, the error criterion function is defined through the modal information as

$$J_2(\boldsymbol{\theta}) = \sum_{i=1}^{M}\left\{\left(\frac{\omega_i - \omega_{di}}{\omega_{di}}\right)^2 + [1 - \mathrm{MAC}(\phi_i, \phi_{di})]\right\} \tag{4}$$

In Eq. (4), ω_i and ω_{di} are the ith natural frequencies of the model and of the damaged system, respectively. Modal assurance criterion (MAC) is a measure of correlation between two sets of mode shapes and is defined as follows[11]:

$$\mathrm{MAC}(\phi_i, \phi_{di}) = \frac{\left|\phi_i^T\phi_{di}^*\right|}{\phi_i^T\phi_i^*\phi_{di}^T\phi_{di}^*} \tag{5}$$

where T denotes matrix transpose and * denotes complex conjugate. By minimizing the error function $J(\boldsymbol{\theta})$ with respect to the damage parameters $\boldsymbol{\theta}$, the extent of damage for those elements that are possibly damaged can be determined.

Received 1 December 1998; revision received 15 May 1999; accepted for publication 19 May 1999.

*Associate Professor, Institute of Aeronautics and Astronautics.
†Graduate Student, Institute of Aeronautics and Astronautics.